Free vibration analysis of simply supported beams with solid and thin-walled cross-sections using higher-order theories based on displacement variables

Free vibration analysis of simply supported beams with solid and thin-walled cross-sections using higher-order theories based on displacement variables

Dan Min[a]*, Alfonso Pagani[b]†, Erasmo Carrera[b]‡

[a]College of Aeronautical Engineering, Civil Aviation University of China, 300300, Tianjin, China.

[b]Department of Mechanical and Aerospace Engineering, Politecnico di Torino, Corso Duca degli Abruzzi 24, 10129 Torino, Italy.

Submitted to

Thin-Walled Structures

Author for correspondence:
E. Carrera, Professor of Aerospace Structures and Aeroelasticity,
Department of Mechanical and Aerospace Engineering,
Politecnico di Torino,
Corso Duca degli Abruzzi 24,
10129 Torino, Italy,
tel: +39 011 090 6836,
fax: +39 011 090 6899,
e-mail: erasmo.carrera@polito.it

*Research Assistant, e-mail: danmincauc@163.com
†Research Assistant, e-mail: alfonso.pagani@polito.it
‡Professor of Aerospace Structures and Aeroelasticity, e-mail: erasmo.carrera@polito.it

ABSTRACT

Solutions for undamped free vibration of beams with solid and thin-walled cross-sections are provided by using refined theories based on displacement variables. In essence, higher-order displacement fields are developed by using the Carrera Unified Formulation (CUF), and by discretizing the cross-section kinematics with bilinear, cubic and fourth-order Lagrange polynomials. Subsequently, the differential equations of motion and the natural boundary conditions are formulated in terms of fundamental nuclei by using CUF and the strong form of the principle of virtual displacements. The second-order system of ordinary differential equations is then reduced into a classical eigenvalue problem by assuming simply-supported boundary conditions. The proposed methodology is extensively assessed for different solid and thin-walled metallic beam structures and the results are compared with those appeared in published literature and also checked by finite element solutions. The research demonstrates that: i) The innovative 1D closed form CUF represents a reliable and compact method to develop refined beam models with solely displacement variables; ii) 3D-like numerically exact solutions of complex structures can be obtained with ease; iii) The numerical efficiency of the present method is uniquely robust when compared to other methods that provide similar accuracies.

1 Introduction

The undamped free vibration analysis of structures has always been a major area of activity in structural design. The results of modal analyses are, in fact, of great interest in dynamic response analyses, acoustics, aeroelasticity and also to avoid resonance. Even today, for a certain class of structures, the most convenient way of conducting modal analyses is by means of idealizing the structure by simplified beam models. Beam models are easy to use and important tools for structural analysts. In aircraft structural design, for example, such models are still widely used in the modelling of helicopter rotor blades, aircraft wings, and propeller blades, amongst others.

The classical and oldest one-dimensional (1D) beam theory is that of Euler [1] and Bernoulli [2], hereinafter referred to as EBBM (Euler-Bernoulli Beam Model), which underwent further developments by Saint-Venant [3, 4] and Timoshenko [5, 6], hereinafter referred to as TBM (Timoshenko Beam Model). As it is well known, the EBBM does not account for transverse shear deformations, while the TBM incorporates a uniform shear distribution along the cross-section of the beam (see more details in [7]). However, these classical beam models haev severe limitations (e.g., the impossibility of dealing with constrained warping and shear-bending couplings). Thus, there are several problems in the engineering practice that cannot be solved with these traditional tools. Deep and thin-walled beams are some examples for which advanced treatment might be necessary.

Many refined beam models can be found in the literature which overcome the shortcomings of classical models. A comprehensive review about existing beam and plate theories was published by Kapania and Raciti [8, 9], who investigated the vibrations, wave propagation, buckling and post-buckling behaviors. Another review about modern theories for beam structures was recently published by Carrera et al. [10]. However, a brief overview about refined 1D models is given here for the sake of completeness. Particular attention should be paid to the pionering works by Sokolnikoff [11] and Timoshenko and Goodier [12]. Gruttmann and his co-workers [13, 14, 15] computed shear correction factors for torsional and flexural shearing stresses in prismatic beams, arbitrary shaped cross-sections as well as wide- and thin-walled structures. The 3D elasticity equations based on Saint-Venant solution were reduced to beam-like structured by Ladevéze et al. [16, 17, 18] for high aspect ratio beams with thin-walled sections. Yu et al. [19, 20, 21] used the variational asymptotic solution of beams to build an asymptotic series. To enhance the description of the normal and shear stress of the beam, El Fatmi [22, 23] introduced improvements of the displacement models over the beam section by introducing a warping function. With the advent of the Finite Element Method (FEM), various beam models were developed for validation purposes and a considerable overview was provided by Reddy [24, 25], whose works discussed both classical and higher-order 1D elements, together with the problem of shear-locking.

As far as the free vibration analysis is concerned, Eisenberger et al. [26] presented a method to compute the exact vibration frequencies of asymmetrical laminated beams. Three higher-order models to analyze the free vibrations of deep fiber reinforced composite beams were addressed by Marur and Kant [27], and the same

authors extended this theory to study vibrations of angle-ply laminated beams by accounting for transverse shear and normal strain effects [28]. A higher order finite element model based on the classical lamination theory was developed by Ganesan and Zabihollah (see [29, 30]), and vibration response from laminated tapered composite beams was subsequently investigated. Kameswara et al. [31] studied a closed form solution with high-order mixed theory for free vibration analysis of composite beams. Numerical examples were computed for beams of various span to height ratios, and the results showed that their theories provide lower natural frequencies than those computed through Timoshenko model in case of thick sandwich beams.

All the publications mentioned above show that refined beam theories and the vibration analysis of slender structures still attract considerable attention of researchers and engineers. The current work presents a new method to deal with the free vibration behavior of beam structures. This method is based on the well-known Carrera Unified Formulation (CUF), which was introduced by Carrera and his co-workers [32, 33, 34] for plates and shells. CUF was extended to beam structures by Carrera and Giunta [35] in 2010. Since then, various improvements of CUF have taken place and a brief overview is given below. The strength of CUF is that it allows the automatic development and compact formulation of any theory of structures by expressing the 3D displacement field as an expansion series of the generalized unknowns, which lie on the beam axis in the case of 1D models, through certain cross-sectional functions (see [7] for a comprehensive discussion about CUF). Several papers in the literature made use of Taylor series polynomials as cross-sectional functions, and the corresponding models were referred to as TE (Taylor Expansion). TE models have demonstrated higher-order capabilities in dealing with various beam problems both in conjunction with FEM methods [36, 37, 38] and exact solutions [39, 40, 41]. More recently, Carrera and Petrolo [42, 43] adopted the Lagrange polynomials to discretize the cross-sectional kinematics and the resulting LE (Lagrange Expansion) CUF models have been successfully used for the analysis of both metallic and laminated composite structures. Some of the main advantages of the LE models are that they only involve pure displacement unknowns and allow the component-wise analysis of complex structures [44].

In the previous literature about LE models, FEM was applied to solve the weak form governing equations. In the present work, for the first time, numerically exact solutions of the strong-form equations of motion of LE models for the free vibration analyses of solid and thin-walled structures are presented by assuming simply supported boundary conditions. The present methodology is said to be exact in the sense that it provides exact solution of the equations of motion of a structure once the initial assumptions on the displacement field have been made.

The paper is organized as follows: i) first, the adopted notation and some preliminary relations are introduced in Section 2; ii) CUF is then presented in Section 3, along with LE models for beams; iii) next, the governing differential equations and natural boundary conditions are derived in Section 4 and 5. Here, by adopting simply supported boundary conditions, the differential problem is reduced into a linear eigenvalue problem in terms of CUF fundamental nuclei; iv) subsequently, a number of significant problems are treated in Section

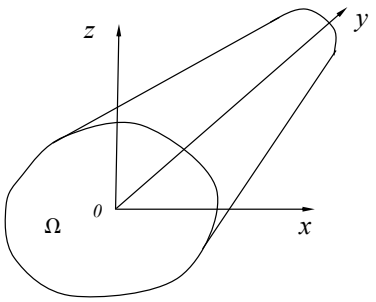

Figure 1: Beam model and related Cartesian frame.

6; v) finally, the main conclusions are outlined.

2 Preliminaries

The coordinate frame of the generic beam model is shown in Fig. 1. The beam has cross-section Ω and length L. The dimensions along y are $0 \leqslant y \leqslant L$. The displacement vector is:

$$\mathbf{u}(x, y, z; t) = \{u_x \; u_y \; u_z\}^{\mathrm{T}} \tag{1}$$

in which u_x, u_y and u_z are the displacement components along x, y and z axis, respectively. The superscript "T" represents a transpose. The stress, $\boldsymbol{\sigma}$, and the strain, $\boldsymbol{\epsilon}$, components are grouped as follows:

$$\boldsymbol{\sigma} = \{\sigma_{yy} \; \sigma_{xx} \; \sigma_{zz} \; \sigma_{xz} \; \sigma_{yz} \; \sigma_{xy}\}^{\mathrm{T}}, \quad \boldsymbol{\epsilon} = \{\epsilon_{yy} \; \epsilon_{xx} \; \epsilon_{zz} \; \epsilon_{xz} \; \epsilon_{yz} \; \epsilon_{xy}\}^{\mathrm{T}} \tag{2}$$

In the case of small displacements with respect to a characteristic dimension in the plane of Ω, the strain-displacement relations are

$$\boldsymbol{\sigma} = \mathbf{D}\mathbf{u} \tag{3}$$

where $\mathbf{D}$ is the following linear differential operator matrix

$$\mathbf{D} = \begin{bmatrix} 0 & \dfrac{\partial}{\partial y} & 0 \\ \dfrac{\partial}{\partial x} & 0 & 0 \\ 0 & 0 & \dfrac{\partial}{\partial z} \\ \dfrac{\partial}{\partial z} & 0 & \dfrac{\partial}{\partial x} \\ 0 & \dfrac{\partial}{\partial z} & \dfrac{\partial}{\partial y} \\ \dfrac{\partial}{\partial y} & \dfrac{\partial}{\partial x} & 0 \end{bmatrix} \tag{4}$$

According to the Hooke's law, the relationship between stress and strain is

$$\boldsymbol{\sigma} = \tilde{\mathbf{C}}\boldsymbol{\epsilon} \tag{5}$$

In the case of isotropic material, the matrix $\tilde{\mathbf{C}}$ is

$$\tilde{\mathbf{C}} = \begin{bmatrix} \tilde{C}_{33} & \tilde{C}_{23} & \tilde{C}_{13} & 0 & 0 & 0 \\ \tilde{C}_{23} & \tilde{C}_{22} & \tilde{C}_{12} & 0 & 0 & 0 \\ \tilde{C}_{13} & \tilde{C}_{12} & \tilde{C}_{11} & 0 & 0 & 0 \\ 0 & 0 & 0 & \tilde{C}_{44} & 0 & 0 \\ 0 & 0 & 0 & 0 & \tilde{C}_{55} & 0 \\ 0 & 0 & 0 & 0 & 0 & \tilde{C}_{66} \end{bmatrix} \tag{6}$$

Coefficients $\tilde{C}_{ij}$ depend on Young's modulus and Poisson's ratio, which can be found in standard texts, see Reddy [25] or Tsai [45].

3 Unified Formulation of beams

Within the framework of CUF (see [7, 46, 47]), the 3D displacement field is expressed as an expansion of the generalized displacements through generic functions F_τ

$$\mathbf{u}(x, y, z; t) = F_\tau(x, z)\mathbf{u}_\tau(y; t) \qquad \tau = 1, 2, ..., M \tag{7}$$

where F_τ varies within the cross-section; $\mathbf{u}_\tau$ is the generalized displacements vector and M stands for the number of terms in the expansion. According to the Einstein notation, the repeated subscript, τ, indicates summation. In this paper, Lagrange polynomials are used for F_τ functions. In particular, four-point (L4) bilinear, nine-point (L9) cubic and 16-point (L16) fourth-order polynomials are used. Fig. 2 shows these elements in the physical plane, and they are all defined on quadrilateral domains. The order of the beam

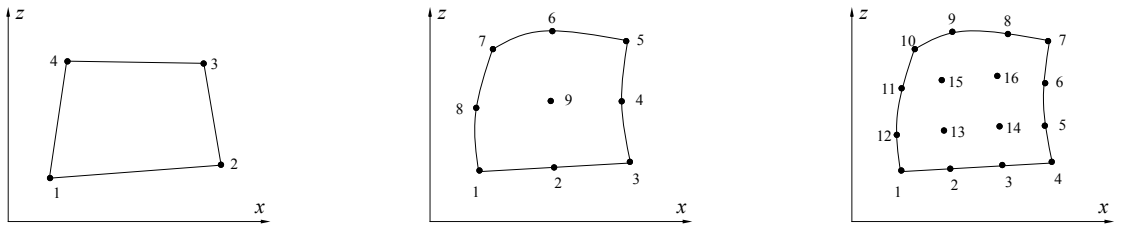

(a) Four-point element, L4 (b) Nine-point element, L9 (c) Sixteen-point element, L16

Figure 2: Lagrange polynomials in actual geometry.

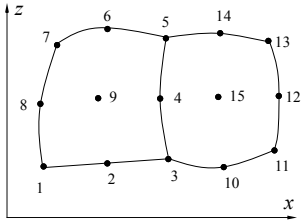

Figure 3: Two assembled L9 elements.

model is directly related to the choice of the F_τ cross-sectional polynomial. Refined models of complex structures can also be implemented by considering cross-sectional assembly of those elements, such as in Fig. 3, where two assembled L9 elements in actual geometry are shown. Moreover, the isoparametric formulation is exploited to do deal with arbitrary shapes.

In the case of the L4 element, the interpolation functions are given by:

$$F_\tau = \frac{1}{4}(1 + \mathrm{r}\ \mathrm{r}_\tau)(1 + \mathrm{s}\ \mathrm{s}_\tau) \qquad \tau = 1, 2, 3, 4 \tag{8}$$

where r and s vary from -1 to $+1$ in the natural plane, and r_τ and s_τ are the coordinates of the four points shown in Fig. 2(a). In the case of an L9 element the interpolation functions are given by:

$$F_\tau = \tfrac{1}{4}(\mathrm{r}^2 + \mathrm{r}\ \mathrm{r}_\tau)(\mathrm{s}^2 + \mathrm{s}\ \mathrm{s}_\tau) \qquad \tau = 1, 3, 5, 7$$

$$F_\tau = \tfrac{1}{2}\mathrm{s}_\tau^2(\mathrm{s}^2 - \mathrm{s}\ \mathrm{s}_\tau)(1 - r^2) + \tfrac{1}{2}\mathrm{r}_\tau^2(\mathrm{r}^2 - \mathrm{r}\ \mathrm{r}_\tau)(1 - \mathrm{s}^2) \qquad \tau = 2, 4, 6, 8 \tag{9}$$

$$F_\tau = (1 - \mathrm{r}^2)(1 - \mathrm{s}^2) \qquad \tau = 9$$

Finally, the L16 polynomials are given by:

$$F_{\tau IJ} = L_I(\mathrm{r})L_J(\mathrm{s}) \qquad I, J = 1, \cdots, 4 \tag{10}$$

where

$$L_1(r) = \frac{1}{16}(\mathrm{r} - 1)(1 - 9\mathrm{r}^2) \quad L_2(\mathrm{r}) = \frac{9}{16}(3\mathrm{r} - 1)(\mathrm{r}^2 - 1)$$

$$L_3(r) = \frac{9}{16}(3\mathrm{r} + 1)(1 - \mathrm{r}^2) \quad L_4(\mathrm{r}) = \frac{1}{16}(\mathrm{r} + 1)(9\mathrm{r}^2 - 1)$$

The complete displacement field of a beam model discretized with one single L9 element is given in the following for illustrative purposes:

$$\begin{aligned} u_x &= F_1 u_{x_1} + F_2 u_{x_2} + F_3 u_{x_3} + F_4 u_{x_4} + F_5 u_{x_5} + F_6 u_{x_6} + F_7 u_{x_7} + F_8 u_{x_8} + F_9 u_{x_9} \\ u_y &= F_1 u_{y_1} + F_2 u_{y_2} + F_3 u_{y_3} + F_4 u_{y_4} + F_5 u_{y_5} + F_6 u_{y_6} + F_7 u_{y_7} + F_8 u_{y_8} + F_9 u_{y_9} \\ u_z &= F_1 u_{z_1} + F_2 u_{z_2} + F_3 u_{z_3} + F_4 u_{z_4} + F_5 u_{z_5} + F_6 u_{z_6} + F_7 u_{z_7} + F_8 u_{z_8} + F_9 u_{z_9} \end{aligned} \tag{11}$$

where $u_{x_1}, ..., u_{z_9}$ are the displacement variables of the problem, and they represent the translational displacement components of each of the nine points of the L9 element.

4 Governing equations

The principle of virtual displacements is used in this paper to derive the equations of motion.

$$\delta L_{\text{int}} = -\delta L_{\text{ine}} \tag{12}$$

where δ stands for a virtual variation operator, L_{int} represents the strain energy, and L_{ine} is the work of the inertial loadings. The virtual variation of the strain energy is

$$\delta L_{\text{int}} = \int_V \delta \boldsymbol{\epsilon}^{\text{T}} \boldsymbol{\sigma} \text{d}V \tag{13}$$

By substitution of the geometrical relations (Eq. (3)), the material constitutive equation (Eq. (5)), and the unified hierarchical approximation of displacements (Eq. (7)), and after integration by parts, Eq. (13) can be rewritten as

$$\delta L_{\text{int}} = \int_L \delta \boldsymbol{u}_\tau^{\text{T}} \mathbf{K}^{\tau s} \boldsymbol{u}_s \text{d}y + \left[\delta \boldsymbol{u}_\tau^{\text{T}} \boldsymbol{\Pi}^{\tau s} \boldsymbol{u}_s \right] |_{y=0}^{y=L} \tag{14}$$

where $\mathbf{K}^{\tau s}$ is the linear differential stiffness matrix and $\boldsymbol{\Pi}^{\tau s}$ is the matrix of natural boundary conditions. For the sake of brevity, these matrices are not given here but they can be found in [40, 41]. The main property of the fundamental nuclei is that their formal mathematical expressions do not depend either on the order of the beam theory or on the choice of F_τ functions.

The virtual variation of the inertial work is given by

$$\delta L_{\text{ine}} = \int_L \int_\Omega \rho \delta \boldsymbol{u}_\tau \ddot{\boldsymbol{u}} \text{d}\Omega \text{d}y \tag{15}$$

where ρ denotes the material density and double over dots stand for the second derivative with respect to time (t). Accounting for Eq. (7), Eq. (15) can be rewritten as

$$\delta L_{\text{ine}} = \int_L \delta \boldsymbol{u}_\tau \int_\Omega \rho F_\tau F_s \mathrm{d}\Omega \ddot{\boldsymbol{u}}_s \mathrm{d}y = \int_L \delta \boldsymbol{u}_\tau \mathbf{M}^{\tau s} \ddot{\boldsymbol{u}}_s \mathrm{d}y \tag{16}$$

where $\mathbf{M}^{\tau s}$ is the 3×3 fundamental, diagonal nucleus of the mass matrix, whose components can be found in [40]. The explicit form of the equations of motion is found by substituting fundamental nuclei into Eq. (12)

$$\begin{aligned}
\delta u_{x\tau} : & - E^{66}_{\tau s} u_{xs_{,yy}} + \left(E^{22}_{\tau_{,x} s_{,x}} + E^{44}_{\tau_{,z} s_{,z}} \right) u_{xs} \\
& + \left(E^{23}_{\tau_{,x} s} - E^{66}_{\tau s_{,x}} \right) u_{ys_{,y}} + \left(E^{44}_{\tau_{,z} s_{,x}} + E^{12}_{\tau_{,x} s_{,z}} \right) u_{zs} = -E^{\rho}_{\tau s} \ddot{u}_{xs} \\
\delta u_{y\tau} : & \left(E^{66}_{\tau_{,x} s} - E^{23}_{\tau s_{,x}} \right) u_{xs_{,y}} - E^{33}_{\tau s} u_{ys_{,yy}} \\
& + \left(E^{66}_{\tau_{,x} s_{,x}} + E^{55}_{\tau_{,z} s_{,z}} \right) u_{ys} + \left(E^{55}_{\tau_{,z} s} - E^{13}_{\tau s_{,z}} \right) u_{zs_{,y}} = -E^{\rho}_{\tau s} \ddot{u}_{ys} \\
\delta u_{z\tau} : & - E^{55}_{\tau s} u_{zs_{,yy}} + \left(E^{44}_{\tau_{,x} s_{,z}} + E^{12}_{\tau_{,z} s_{,x}} \right) u_{xs} \\
& + \left(E^{13}_{\tau_{,z} s} - E^{55}_{\tau s_{,z}} \right) u_{ys_{,y}} + \left(E^{44}_{\tau_{,x} s_{,x}} + E^{11}_{\tau_{,z} s_{,z}} \right) u_{zs} = -E^{\rho}_{\tau s} \ddot{u}_{zs}
\end{aligned} \tag{17}$$

The generic term $E^{\alpha\beta}_{\tau_{,\theta} s_{,\zeta}}$ above is a cross-sectional moment parameter

$$E^{\alpha\beta}_{\tau_{,\theta} s_{,\zeta}} = \int_\Omega \tilde{C}_{\alpha\beta} F_{\tau_{,\theta}} F_{s_{,\zeta}} \mathrm{d}\Omega \tag{18}$$

The suffix after the comma denotes the derivatives. Moreover,

$$E^{\rho}_{\tau s} = \int_\Omega \rho F_\tau F_s \mathrm{d}\Omega \tag{19}$$

Letting $\mathbf{P}_\tau = \{P_{x\tau} \quad P_{y\tau} \quad P_{z\tau}\}^{\mathrm{T}}$ to be the vector of the generalized forces, the natural boundary conditions are

$$\begin{aligned}
\delta u_{x\tau} : P_{xs} &= E^{66}_{\tau s} u_{xs_{,y}} + E^{66}_{\tau s_{,x}} u_{ys} \\
\delta u_{y\tau} : P_{ys} &= E^{23}_{\tau s_{,x}} u_{xs} + E^{33}_{\tau s} u_{ys_{,y}} + E^{13}_{\tau s_{,z}} u_{zs} \\
\delta u_{z\tau} : P_{zs} &= E^{55}_{\tau s_{,z}} u_{ys} + E^{55}_{\tau s} u_{zs_{,y}}
\end{aligned} \tag{20}$$

5 Analytical solution of the strong-form governing equations

By imposing simply supported boundary conditions, the above differential equations can be solved in analytical form. For doing this, the following generalized displacements, which correspond to a Navier-type solution, are supposed:

$$u_{xs}(y;t) = \phi_{xs} \sin(\alpha y) e^{i\omega t}$$

$$u_{ys}(y;t) = \phi_{ys}\cos(\alpha y)e^{i\omega t} \tag{21}$$

$$u_{zs}(y;t) = \phi_{zs}\sin(\alpha y)e^{i\omega t}$$

Where α is:

$$\alpha = \frac{m\pi}{L} \tag{22}$$

and m is a positive integer, which represents the half waves number along the beam axis and i is the imaginary unit. The components of vector $\boldsymbol{\phi}_s = \{\phi_{xs}\ \phi_{ys}\ \phi_{zs}\ \}^{\mathrm{T}}$ are the new unknown parameters. The displacement field in Eq. (21) satisfies a natural boundary condition along the cross-section directions and a mechanical one along the axial direction.

After substituting Eq. (21) into the governing equations (17), the fundamental nucleus of the algebraic eigensystem is obtained:

$$\delta\phi_\tau : (\bar{\mathbf{K}}^{\tau s} - \omega^2\bar{\mathbf{M}}^{\tau s})\boldsymbol{\phi}_s = 0 \tag{23}$$

$\bar{\mathbf{K}}^{\tau s}$ and $\bar{\mathbf{M}}^{\tau s}$ are the fundamental nuclei of the algebraic stiffness and mass matrices, respectively. The components of the linear stiffness matrix $\bar{\mathbf{K}}^{\tau s}$ are

$$\begin{aligned}
K_{xx}^{\tau s} &= \alpha^2 E_{\tau s}^{66} + E_{\tau_{,x} s_{,x}}^{22} + E_{\tau_{,z} s_{,z}}^{44} \\
K_{xy}^{\tau s} &= \alpha\left(E_{\tau_{,x} s}^{23} - E_{\tau s_{,x}}^{66}\right) \\
K_{xz}^{\tau s} &= E_{\tau_{,z} s_{,x}}^{44} + E_{\tau_{,x} s_{,z}}^{12} \\
K_{yx}^{\tau s} &= \alpha\left(E_{\tau_{,x} s}^{66} - E_{\tau s_{,x}}^{23}\right) \\
K_{yy}^{\tau s} &= \alpha^2 E_{\tau s}^{33} + E_{\tau_{,x} s_{,x}}^{66} + E_{\tau_{,z} s_{,z}}^{55} \\
K_{yz}^{\tau s} &= \alpha\left(E_{\tau_{,z} s}^{55} - E_{\tau s_{,z}}^{13}\right) \\
K_{zx}^{\tau s} &= E_{\tau_{,x} s_{,z}}^{44} + E_{\tau_{,z} s_{,x}}^{12} \\
K_{zy}^{\tau s} &= \alpha^2 E_{\tau s}^{55} + \alpha\left(E_{\tau_{,z} s}^{13} - E_{\tau s_{,z}}^{55}\right) \\
K_{zz}^{\tau s} &= E_{\tau_{,x} s_{,x}}^{44} + E_{\tau_{,z} s_{,z}}^{11}
\end{aligned} \tag{24}$$

whereas the components of $\bar{\mathbf{M}}^{\tau s}$ are

$$\begin{aligned}
M_{xx}^{\tau s} &= M_{yy}^{\tau s} = M_{zz}^{\tau s} = E_{\tau s}^{\rho} \\
M_{xy}^{\tau s} &= M_{xz}^{\tau s} = M_{yx}^{\tau s} = M_{yz}^{\tau s} = M_{zx}^{\tau s} = M_{zy}^{\tau s} = 0
\end{aligned} \tag{25}$$

For a fixed approximation order and cross-sectional LE discretization, the eigensystem is automatically expanded according to the summation indexes τ and s.

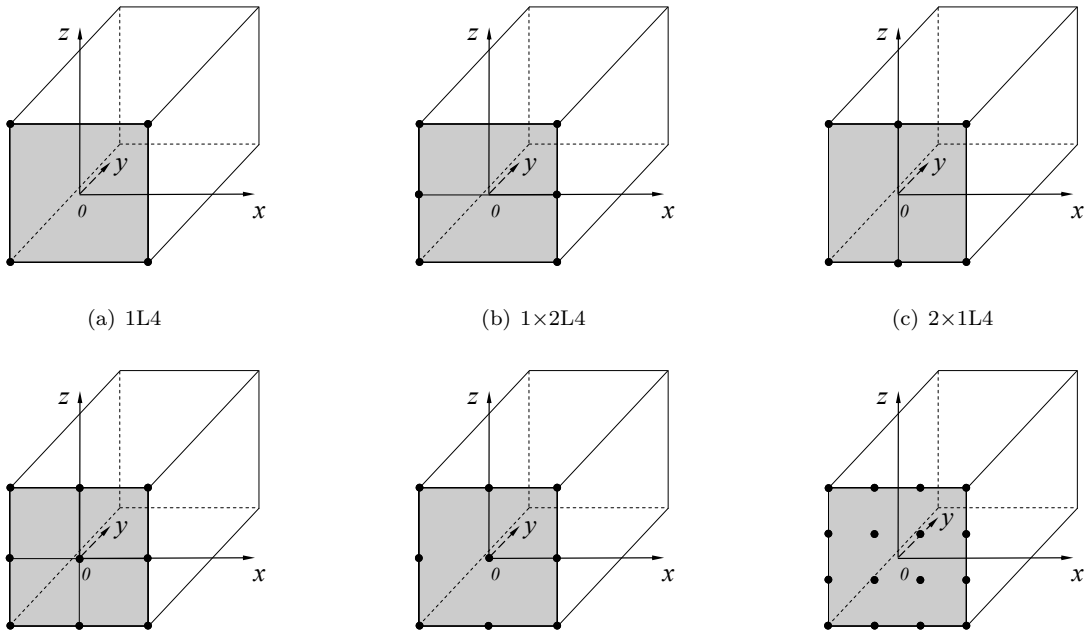

(a) 1L4 (b) 1×2L4 (c) 2×1L4

(d) 2×2L4 (e) 1L9 (f) 1L16

Figure 4: LE modelling of the square cross-section beam.

6 Numerical results

The present refined 1D model is compared and evaluated here by analyzing different problems. The results from the LE strong-form solutions are compared with those from classical beam models (EBBM and TBM) and 3D solid models by using the commercial code MSC Nastran. MSC Nastran models are based on HEXA-8 brick elements [48]. All of those models have the same boundary condition that is simply supported at both sides ($y = 0, L$).

6.1 Square cross-section beams

Square cross-section beams are considered for preliminary assessments. The beam has a square cross-section ($a = b$), with $b = 0.2$ m. Two different slenderness ratios, L/b, are considered: 10 and 100. The isotropic material data are: Young modulus, $E = 75$ GPa; Poisson ratio, $\nu = 0.33$, material density $\rho = 2700$ kg/m^3. Table 1 shows the first ten non-dimensional natural frequencies $\omega^* = (\omega L^2/b)\sqrt{\rho/E}$ for simply-supported beam with $L/b = 10$. The results from the present LE models are compared to those from classical theories (EBBM, TBM) from Ref. [40]. In Table 1, m represents the number of semi-waves as described in Eq. (22). Various LE models are considered in the table and they are shown in rows 4 to 9. The LE cross-sectional discretizations with Lagrange elements are depicted in Fig. 4 for the problem under consideration. Unless differently specified, "1" in "1 × 2L4" stands for the number of L4 elements along the ox direction, and "2" is the number of L4 elements along the oz direction. The comparison of the results in Table 1 shows the correctness of the present strong-form LE beam. Even the most simple one, 1L4 with a number of degrees of

Table 1: First ten non-dimensional flexural frequencies $\omega^* = (\omega L^2/b)\sqrt{\rho/E}$ for simply-supported beam, $L/b = 10$

Model	DOFs	m=1	2	3	4	5	6	7	8	9	10
EBBM [40]	6	2.838	11.213	24.742	42.847	64.869	90.330	117.859	147.586	178.779	211.040
TBM [40]	10	2.807	10.779	22.847	37.858	54.856	73.192	92.334	112.049	132.111	152.388
Current theory											
1L4	12	3.063	11.704	24.653	40.573	58.415	77.456	97.226	117.424	137.862	158.418
$1 \times$ 2L4	18	2.914	11.168	23.617	39.030	56.416	75.074	94.536	114.499	134.763	155.196
$2 \times$ 1L4	18	2.998	11.474	24.213	39.923	57.575	76.452	96.083	116.166	136.509	156.989
$2 \times$ 2L4	27	2.839	10.890	23.055	38.143	55.187	73.500	92.621	112.248	132.183	152.299
1L9	27	2.808	10.784	22.869	37.902	54.929	73.268	92.453	112.178	132.240	152.506
1L16	48	2.803	10.722	22.618	37.291	53.794	71.472	89.898	108.799	127.998	147.383

Table 2: First four non-dimensional flexural frequencies $\omega^* = (\omega L^2/b)\sqrt{\rho/E}$ for simple-supported beam, $L/b = 100$

Model	m=1	2	3	4
EBBM [40]	2.859	11.535	26.359	47.891
TBM	2.856	11.531	26.330	47.800
Refined-TE [40]	2.859	11.552	26.442	48.161
Current theory				
1L4	3.113	12.449	27.988	49.967
$1 \times$ 2L4	3.008	12.024	27.034	48.005
$2 \times$ 1L4	2.921	11.679	26.256	46.626
$2 \times$ 2L4	2.881	11.521	25.904	46.001
1L9	2.812	11.245	25.282	44.899
1L16	2.812	11.244	25.278	44.626

freedom (DOFs) equal to 12, shows its convergence with respect to EBBM. Attention should be paid to $1 \times$2L4 and $2 \times$1L4, which are different models, and thus presenting different behavior in the flexure directions along ox and oz. Though the $2 \times$ 2L4 model of Fig. 4(d) has the same number of DOFs as 1L9, the latter presents slightly more precise results, at least in the range of the lower frequencies. The results of the 16L9 model show the higher-interpolation, fourth-order capabilities, owning the best accuracy, which is particularly evident in the higher frequencies range. Similar conclusions can be extrapolated from the results of the slender beam ($L/b = 100$) shown in Table 2, where also the higher-order TE models from Ref. [40] are given for comparison purposes. The first six different modes for m=1 and L/b=10 are shown in Fig. 5. In particular, flexural, torsional, extensional and shear modes are shown. Those figures clearly demonstrate the 3D capabilities of the present beam formulation.

6.2 C-shaped cross-section beam

A C-shaped beam is another example considered for the assessment of the present beam model. The geometry of the cross-section is shown in Fig. 6(a). The sides of the cross-section are $a = 0.2$ m and $b = a$. The thicknesses of the flanges are $t = a/10$, and the length-to-side ratio $L/a = 10$. The material data are: Young modulus, $E = 198$ GPa; Poisson ratio, ν, equals to 0.3, material density $\rho = 7850$ kg/m^3. Various order LE models are considered in the following analysis and some cross-sectional discretizations are shown in Figs. 6(b) to 6(f) for illustrative purposes.

Table 3 shows the first modes corresponding to m=1 to m=8. Results in rows 3 to 9 are those from the

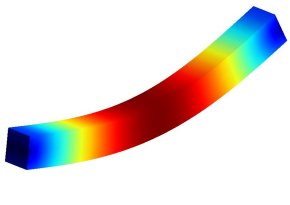

(a) Flexural mode along z, $\omega^* = 2.80$

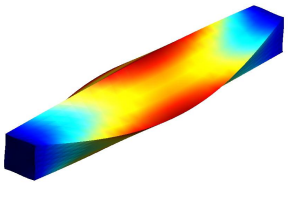

(b) Torsional mode, $\omega^* = 17.70$

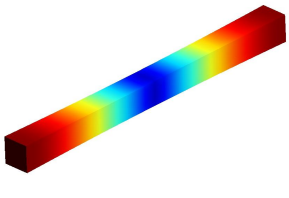

(c) Axial mode, $\omega^* = 31.38$

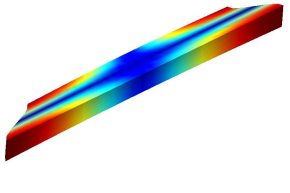

(d) Shear mode in yz plane, $\omega^* = 195.66$

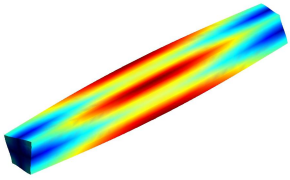

(e) 45° tensile mode along y, $\omega^* = 243.75$

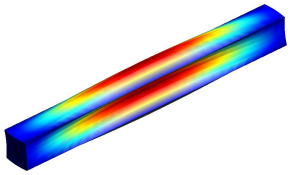

(f) Tensile mode along z, $\omega^* = 273.08$

Figure 5: Selected mode shapes of the square cross-section beam by the 1L16 model and m=1.

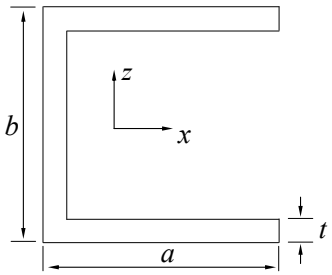

(a) C-shaped cross-section

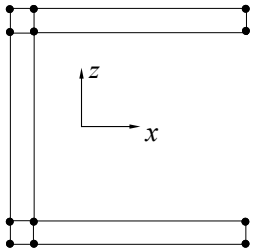

(b) 5L4

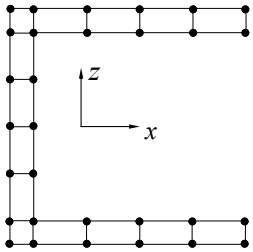

(c) 14L4

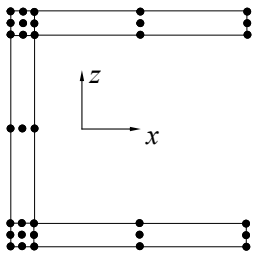

(d) 5L9

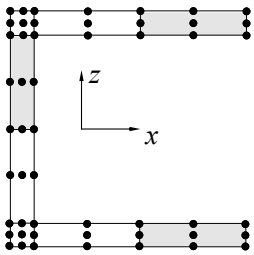

(e) 8L9

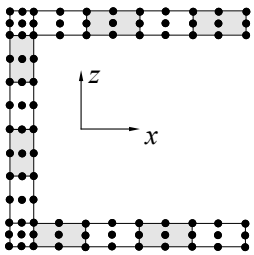

(f) 14L9

Figure 6: C-shaped cross-section and LE discretizations.

Table 3: First frequencies(Hz) related to m=1 to 8 of the C-shaped cross-section beam

Cross-section		Natural Frequencies							
Model	DOFs	m=1	2	3	4	5	6	7	8
5L4	36	71.399	125.190	230.710	269.411	966.524[(a)]	978.398	461.403	1011.057[(b)]
8L4	54	70.237	123.167	225.165	267.958	670.719	689.362	443.164	719.209
14L4	90	69.700	122.510	220.824	267.473	457.367	490.185	417.933	530.673
26L4	162	69.397	122.325	217.426	267.282	363.843	394.424	396.893	453.183
5L9	99	69.360	122.256	218.971	267.083	314.102	350.559	409.009	414.622
8L9	153	69.158	122.173	215.103	266.894	300.941	339.205	383.042	404.349
14L9	261	68.995	122.149	214.018	266.780	297.059	335.286	377.374	400.022
3D FEM coarse	20793	69.019	122.172	213.841	266.065	295.383	333.546	376.303	397.905
3D FEM finer	101238	68.894	122.152	213.405	266.418	293.450	331.633	374.324	395.995

[(a)] Percentage difference from 3D FEM coarse model is 227.2%.
[(b)] Percentage difference from 3D FEM coarse model is 154.1%.

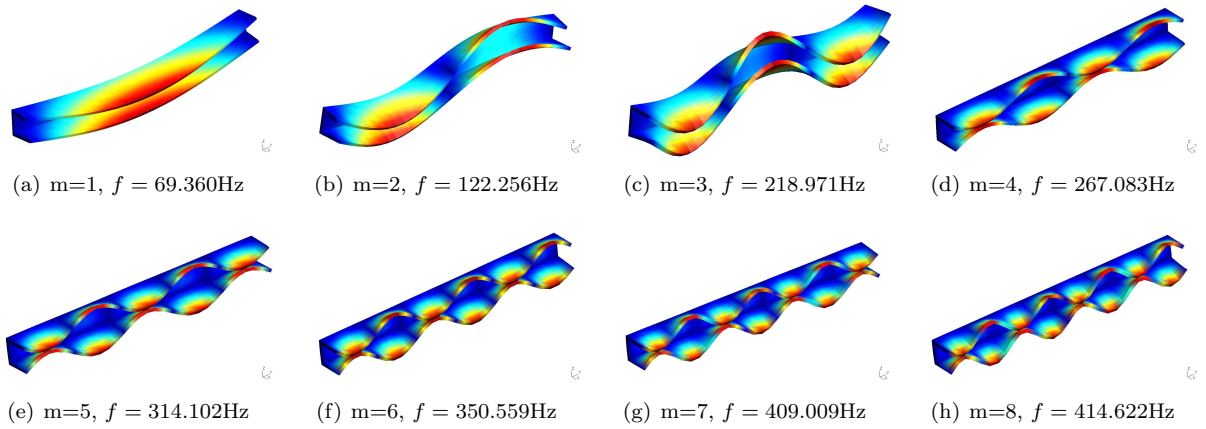

(a) m=1, $f = 69.360$Hz (b) m=2, $f = 122.256$Hz (c) m=3, $f = 218.971$Hz (d) m=4, $f = 267.083$Hz

(e) m=5, $f = 314.102$Hz (f) m=6, $f = 350.559$Hz (g) m=7, $f = 409.009$Hz (h) m=8, $f = 414.622$Hz

Figure 7: First modes related to $m = 1$ to 8 of C-shaped cross-section by the 5L9 model.

present beam models, whereas those in rows 10 and 11 come from MSC Nastran solid solutions. L4 models from 5 to 26 elements, and L9 models from 5 to 14 elements prove the accuracy of the proposed solution. The results from columns 3 to 6 show that both L4 and L9 models are affected by errors that are lower then 3% with respect to the 3D FEM solutions. On the other hand, considerable errors are produced by lower-order beam models in the higher frequencies range. The reason lower order L4 models do not give good results is that models from 5L4 to 14L4 do not have enough DOFs to characterize the shell-like modes. This aspect is clarified from Fig. 7, which shows the modes of vibrations by the 5L9 model. The first modes related to m=1 to 3 (see (Fig. 7(a) to 7(c)) are flexural mode, while all the later modes (Fig. 7(d) to 7(h)) show the complex modes.

6.3 Z-shaped cross-section beam

Next, a Z-shaped beam is considered to asses the present beam model for thin-walled structural analysis. The dimensions of the cross-section are shown in Fig. 8(a). The height of the cross-section is $b = 0.3$ m, and the length of horizontal flange is $a = 0.2$ m. The thickness of the both flange is $t = 0.05$ m, and the length-to-side ratio is $L/a = 10$. The material data are: Young modulus, $E = 206$ GPa; Poisson ratio, $\nu = 0.3$, material

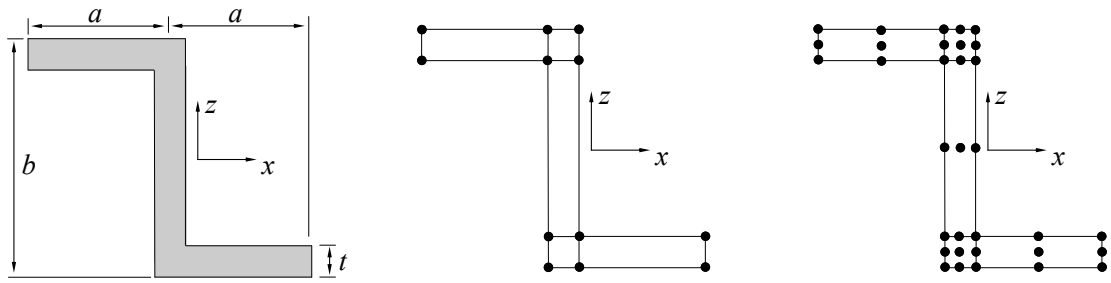

(a) Z-shaped cross-section

(b) 5L4

(c) 5L9

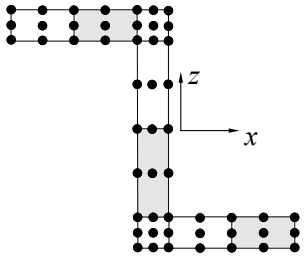

(d) 8L9

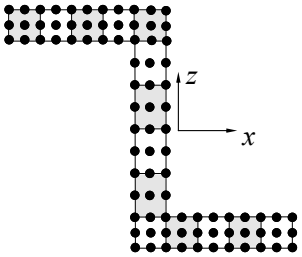

(e) 14L9

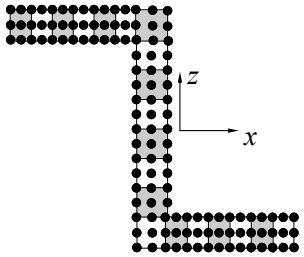

(f) 20L9

Figure 8: Z-shaped cross-section and related LE discretizations.

density $\rho = 7800$ kg/m^3. The previous examples proved that the L9 models provide better convergence with respect to the L4 models. Hence, mainly L9 theories are considered in the following analysis and the related discretizations of the Z-section beam are shown in Figs. 8(b) to 8(f).

The first eight frequencies related to m=1 to 5 are shown in Table 4 for simply supported boundary conditions. The results from the current LE 1D models are compared to solutions obtained by MSC Nastran 3D FEM models. The results indicated that some modes are lost if lower-order beam models are employed. The reason is that, in those models, the number of DOFs is not enough to characterize all the modes under consideration. This aspect is further underlined by considering, for example, the third mode related to m=1. This mode shape by various models is shown in Fig. 8. It is clear that the mode shapes by the present refined models progressively approaches the one by the 3D FEM model as the number of cross-sectional elements (thus, the beam theory order) is increased. In particular, for this particular case, at least 14 L9 elements should be used for correctly describing that mode.

6.4 I-shaped cross-section beam

The analysis of a simply-supported I-section beam is now carried out to illustrate the method. The geometry of the cross-section is shown in Fig. 10(a). The dimensions of the beam are as follow: The height of the cross-section is $b = 0.1$ m, width $a = 0.096$ m. The thicknesses of the flanges are $t_1 = 0.008$ m, thickness of the web $t_2 = 0.005$ m, the length-to-height ratio, $L/b = 10$. The material data are: Young modulus, $E = 210$ GPa; Poisson ratio, $\nu = 0.29$, material density $\rho = 2700$ kg/m^3. The cross-sectional discretization of LE

Table 4: Natural frequencies (Hz) of the Z-shaped beam for m=1 to 5

Cross-section			Natural Frequencies							
Seq.	Model	DOFs	Mode:1	2	3	4	5	6	7	8
	5L4	36	44.368	58.534	–[(a)]	719.389	–	–	–	–
	5L9	99	41.010	53.281	59.056	173.600	–	391.782	2176.989	–
	8L9	153	41.520	53.663	55.449	117.320	161.118	395.659	647.466	-
m=1	14L9	261	41.274	52.574	54.002	105.180	158.984	293.680	534.991	703.450
	20L9	369	41.251	52.410	53.909	104.109	158.884	284.536	521.673	671.256
	3D FEM coarse	12906	41.212	52.142	53.756	103.484	158.247	279.925	509.420	650.632
	3D FEM finer	23694	41.219	52.191	53.781	103.418	158.440	279.238	510.347	650.468
	5L4		–	–	–	732.832	–	–	–	–
	5L9		64.462	134.809	160.230	273.324	375.722	553.470	–	–
	8L9		60.908	94.670	163.837	261.458	378.984	559.558	656.044	1271.271
m=2	14L9		59.529	83.485	156.694	260.625	303.354	516.701	541.856	738.450
	20L9		59.422	82.474	155.340	260.150	297.198	509.468	528.760	712.420
	3D FEM coarse		59.125	81.668	155.093	259.917	293.279	505.566	515.900	692.994
	3D FEM finer		59.206	81.691	154.807	259.848	293.117	505.033	517.159	694.144
	5L4		–	419.017	–	–	–	–	–	–
	5L9		73.782	149.567	293.908	464.581	–	–	–	–
	8L9		69.893	102.818	297.799	466.914	519.335	682.304	1009.850	1293.810
m=3	14L9		68.625	91.478	236.074	438.278	502.313	580.156	686.635	1049.965
	20L9		68.513	90.437	229.188	436.271	493.973	571.055	658.797	945.824
	3D FEM coarse		68.156	89.526	226.727	432.444	490.572	559.334	643.808	910.461
	3D FEM finer		68.273	89.594	225.885	433.253	489.308	561.281	642.720	900.159
	5L4		509.337	534.289	–	–	–	–	–	–
	5L9		85.698	158.798	341.034	699.013	–	–	–	–
	8L9		81.547	111.793	343.639	631.195	703.551	903.008	1292.319	1525.508
m=4	14L9		80.369	101.018	257.116	551.129	608.967	819.528	821.236	1140.731
	20L9		80.246	99.992	248.879	538.003	591.373	779.448	806.721	1073.830
	3D FEM coarse		79.803	98.965	245.407	526.295	576.196	761.658	801.493	1050.311
	3D FEM finer		79.965	99.098	244.666	527.234	577.433	755.580	800.121	1047.180
	5L4		547.636	571.312	–	–	–	–	–	–
	5L9		100.079	169.359	359.985	–	–	–	–	–
	8L9		95.795	123.165	361.836	659.777	953.892	1211.315	1391.537	1627.873
m=5	14L9		94.656	113.047	270.442	568.658	662.719	947.787	1123.155	1424.357
	20L9		94.510	112.033	261.873	555.652	636.449	859.257	1113.908	1405.704
	3D FEM coarse		93.957	110.864	257.806	542.392	616.030	828.336	1111.800	1393.400
	3D FEM finer		94.172	111.070	257.270	544.060	617.660	819.250	1107.600	1377.180

[(a)] Mode not provided by this model.

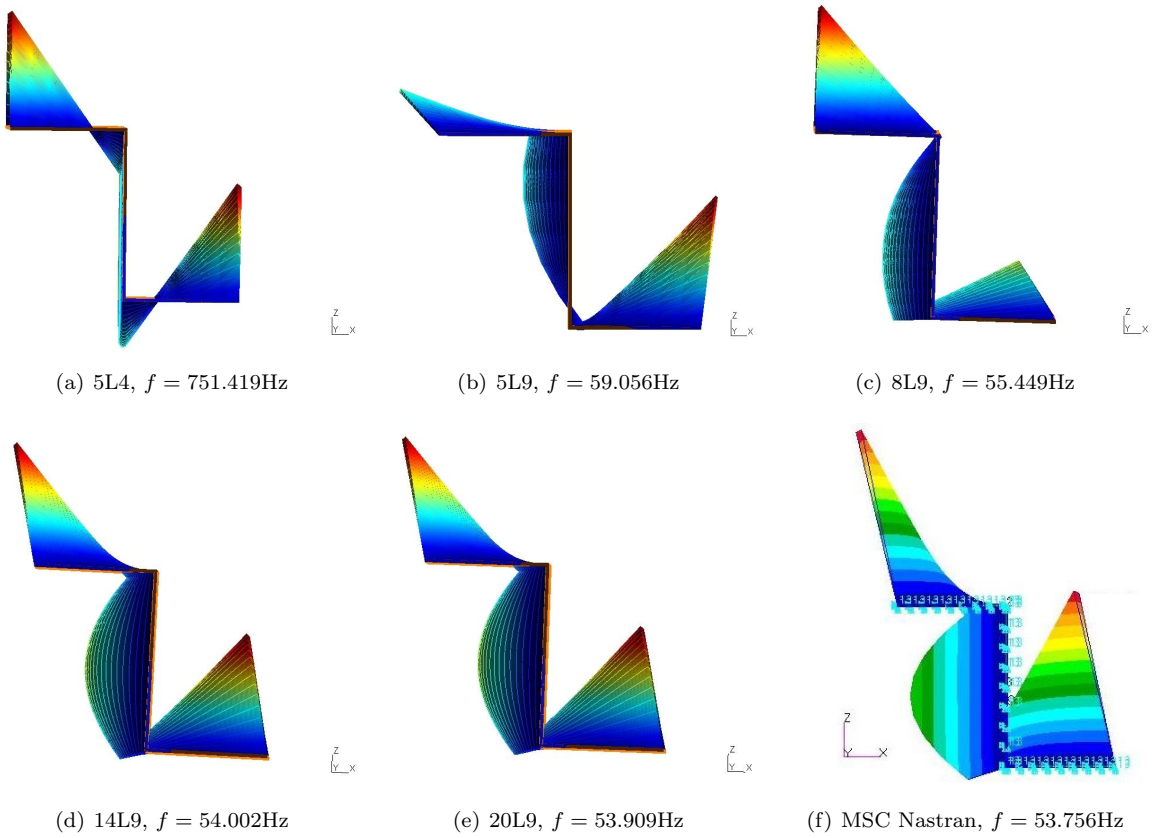

(a) 5L4, $f = 751.419$Hz (b) 5L9, $f = 59.056$Hz (c) 8L9, $f = 55.449$Hz

(d) 14L9, $f = 54.002$Hz (e) 20L9, $f = 53.909$Hz (f) MSC Nastran, $f = 53.756$Hz

Figure 9: Third mode of m=1 by different beam models and 3D FEM; cross-sectional view.

models are shown from Figs. 10(b) to 10(e).

Table 5 shows the first eight frequencies from m=1 to 5 by the current theory and various beam approximations. For the sake of brevity, only one MSC Nastran model is introduced for comparison. Only the flanges of the I-shaped beam are subjected to flexure in the 7L4 model, whereas both the web and the flanges are subjected to flexure in the L9 model if m=2. From m=3, the first mode according to the 7L4 model is torsional, and those of the L9 models are shell-like. For higher number of half-waves along y (m=3 to m=5), the 7L9 beam is not able to correctly catch some mode shapes. Also, for those lower-order models, the 7th and 8th modes for m=3 interchange their order of appearance. In fact, these two modes are both torsional according to the 22L9 beam and the 3D MSC Nastran solution, with the 7th mode characterized by displacements mainly along the axis x and the 8th one mainly along z, respectively. For clarity purposes, Fig. 11 shows the first eight modes by the 22L9 beam model.

6.5 Single-bay box beam

In this section, a single-bay box beam is investigated and it is shown in Fig. 12, where both geometry and cross-sectional LE discretizations are depicted. The height of the cross-section is $a = 0.2$ m, with $a = b$. The thickness of the wall is $t = a/10$. The material data are: Young modulus, $E = 75$ GPa; Poisson ratio, ν, equals to 0.3, material density $\rho = 2700$ kg/m^3.

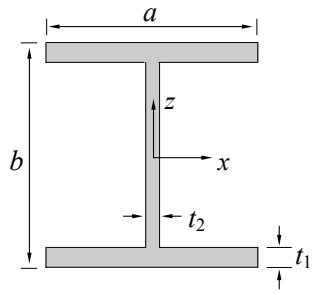

(a) I-shaped cross-section

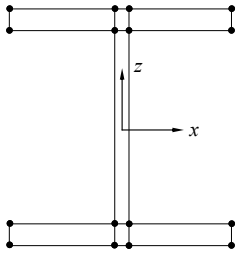

(b) 7L4

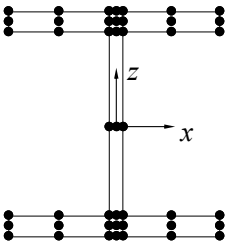

(c) 7L9

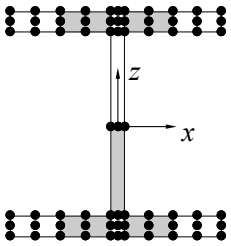

(d) 12L9

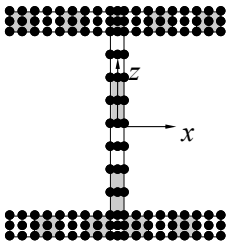

(e) 22L9

Figure 10: Cross-section geometry of the I-shaped cross-section and LE discretizations.

Table 5: Natural frequencies (Hz) of the I-shaped beam for m=1 to 5

Cross-section			Natural Frequencies							
Seq.	Model	DOFs	Mode:1	2	3	4	5	6	7	8
	7L4	48	339.545	404.054	534.931	–[(a)]	–	4404.958	11981.162	–
	7L9	135	335.393	398.418	531.544	1006.605	4402.992	4768.999	6075.132	8368.625
m=1	12L9	225	335.313	396.996	530.914	994.562	2107.921	4401.035	5347.278	7381.452
	22L9	405	335.243	395.864	530.614	991.674	1931.450	4400.280	5219.536	7160.785
	3D FEM	29158	335.280	395.402	530.932	983.823	1904.033	4399.897	5187.244	6789.857
	7L4		–	1322.189	–	1737.646	7723.078	12042.218	–	20885.507
	7L9		1204.251	1301.128	1372.452	1701.154	4871.676	6122.432	8586.663	8812.446
m=2	12L9		1195.930	1284.084	1366.463	1688.659	2322.153	5402.932	7622.712	8807.078
	22L9		1190.180	1277.051	1363.527	1684.414	2164.859	5273.986	7212.408	7476.421
	3D FEM		1187.361	1273.131	1358.823	1686.704	2140.894	5239.671	6838.959	7380.689
	7L4		–	2694.518	–	3113.556	–	11741.815	–	21466.107
	7L9		1628.429	2592.602	2775.070	2948.561	5174.825	6231.728	14489.678	9153.479
m=3	12L9		1613.401	2166.378	2766.058	2888.097	3180.344	5519.599	11395.208	8249.554
	22L9		1601.949	2074.220	2744.869	2870.784	3125.249	5388.937	7347.474	8114.873
	3D FEM		1594.985	2052.998	2741.008	2873.976	3119.626	5350.964	6973.217	8010.766
	7L4		–	4292.199	4464.659	–	–	5762.790	–	–
	7L9		2056.840	3824.460	4023.358	4574.167	6010.969	6382.989	14688.695	–
m=4	12L9		2038.891	2614.677	3871.485	4534.925	4949.135	5683.270	11598.440	–
	22L9		2022.547	2499.851	3832.124	4405.930	4929.413	5550.587	7673.970	9141.949
	3D FEM		2013.938	2473.962	3830.531	4377.397	4928.977	5507.521	7319.556	9030.419
	7L4		–	5721.529	5730.492	5954.518	–	–	21087.415	–
	7L9		2528.014	4549.770	4879.633	6580.620	–	–	11257.629	–
m=5	12L9		2506.481	3040.175	4622.847	5896.662	6432.015	7067.989	10575.939	19976.870
	22L9		2484.621	2928.238	4560.055	5761.649	5844.220	7048.460	10474.928	17875.399
	3D FEM		2473.380	2899.938	4548.228	5701.437	7047.545	8280.360	10355.600	16630.220

[(a)] Mode not provided by this model.

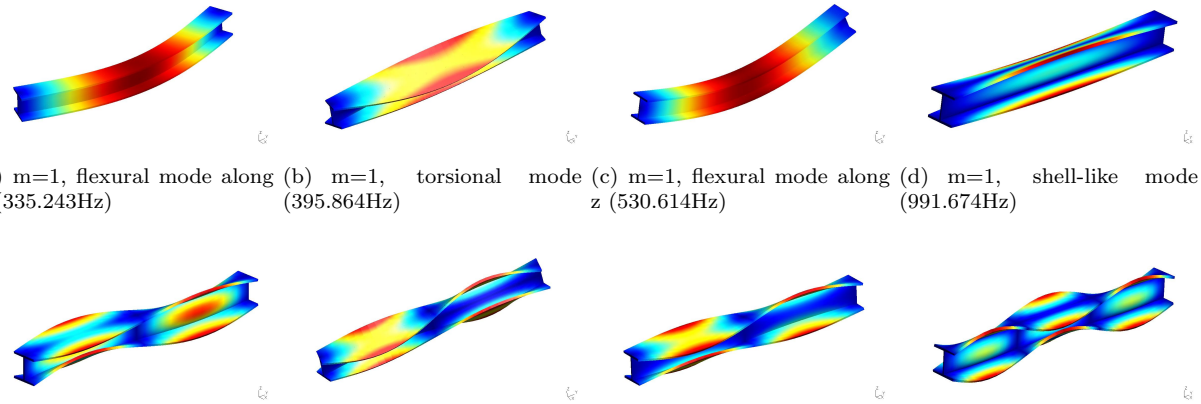

(a) m=1, flexural mode along x (335.243Hz) (b) m=1, torsional mode (395.864Hz) (c) m=1, flexural mode along z (530.614Hz) (d) m=1, shell-like mode (991.674Hz)

(e) m=2, shell-like including web deformation (1190.180Hz) (f) m=2,torsional mode(1277.051Hz) (g) m=2, shell-like with no web deformation (1363.527Hz) (h) m=3, shell-like with web deformation (1502.888Hz)

Figure 11: First eight modes of the I-shaped cross-section beam by the 22L9 model.

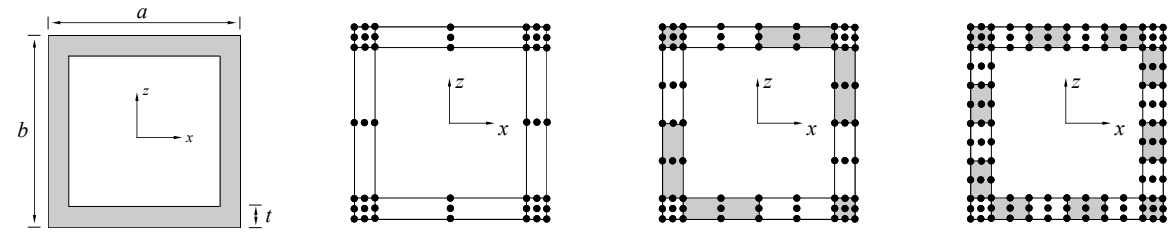

(a) Single box cross-section (b) 8L9 (c) 12L9 (d) 20L9

Figure 12: Single-bay box beam and related LE models.

Table 6: Natural frequencies(Hz) of the single-bay box beam for m=1 to 5

Cross-section			Natural Frequencies							
Seq.	Model	DOFs	Mode:1	2	3	4	5	6	7	8
	8L4	48	148.987	148.987	735.824	2723.141	1316.097	–[(a)]	–	–
	8L9	144	147.057	147.057	732.476	1783.628	1315.958	1607.782	4843.906	4843.906
m=1	12L9	216	146.948	146.948	726.936	1024.797	1315.923	1568.297	3450.389	3450.389
	20L9	360	146.894	146.894	724.519	966.028	1315.881	1524.449	3095.744	3095.744
	3D FEM	86160	146.900	146.900	723.710	949.664	1315.840	1519.767	3040.238	3040.238
	8L4		541.657	541.657	–	1471.897	–	2622.368	–	–
	8L9		531.253	531.253	–	1464.628	1642.901	2620.366	5095.017	5095.017
m=2	12L9		528.747	528.747	1085.567	1450.540	1604.044	2618.608	3465.713	3465.713
	20L9		527.571	527.571	1031.094	1445.249	1560.901	2615.398	3119.434	3119.434
	3D FEM		527.554	527.554	1015.517	1443.544	1555.720	2614.349	3064.061	3064.061
	8L4		1078.284	1078.284	2783.294	–	2208.465	–	–	–
	8L9		1045.865	1045.865	1923.669	–	2196.130	5317.571	5317.571	6436.292
m=3	12L9		1030.235	1030.235	1277.072	1663.646	2166.984	3555.632	3555.632	3854.724
	20L9		1023.011	1023.011	1232.419	1621.573	2157.789	3221.015	3221.015	3626.434
	3D FEM		1022.372	1022.372	1219.150	1615.550	2154.979	3165.353	3165.353	3549.793
	8L4		1685.754	1685.754	2949.072	–	2945.768	–	–	–
	8L9		1607.426	1607.426	2176.254	1783.860	2926.655	5518.367	5518.367	6613.879
m=4	12L9		1552.390	1552.390	1626.795	1747.112	2871.361	3740.112	3740.112	4550.453
	20L9		1527.130	1527.130	1593.379	1706.349	2856.392	3428.984	3428.984	3752.919
	3D FEM		1523.729	1523.729	1582.976	1699.131	2852.047	3374.227	3374.227	3646.819
	8L4		–	2324.809	2324.809	3241.260	3684.039	–	–	–
	8L9		1889.914	2163.547	2163.547	2571.319	3655.870	5747.241	5747.241	5789.197
m=5	12L9		1854.414	2025.241	2025.241	2102.983	3556.948	4038.622	4038.622	4671.210
	20L9		1815.065	1964.550	1964.550	2078.136	3533.063	3769.040	3769.040	3813.034
	3D FEM		1806.292	1954.589	1954.589	2070.038	3526.294	3718.016	3718.016	3798.016

[(a)] Mode not provided by this model.

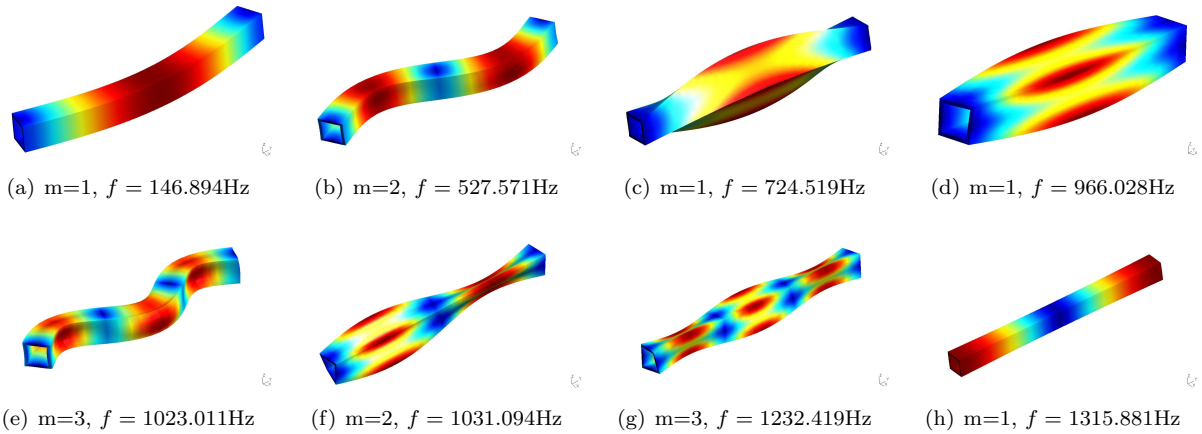

(a) m=1, $f = 146.894$Hz (b) m=2, $f = 527.571$Hz (c) m=1, $f = 724.519$Hz (d) m=1, $f = 966.028$Hz

(e) m=3, $f = 1023.011$Hz (f) m=2, $f = 1031.094$Hz (g) m=3, $f = 1232.419$Hz (h) m=1, $f = 1315.881$Hz

Figure 13: First eight modes of the single box cross-section by the 20L9 model.

Compared with the L4 results from Z-shaped and I-shaped cross-section beams, the proposed 1D models of the single-bay box provide better results as shown in Table 6. As the symmetric boundary conditions (simple supported beam on both sides) and cross-section, some natural frequencies can be found twice in this table (see mode 1 and mode 2 from m=1 to m=4). Given the same number of cross-sectional elements, namely 8, the L4 and L9 beam models provide quite different results. Some modes in L4 are, in fact, missing because of the lower number of DOFs. Some frequencies (see mode 4 in m=1; mode 3 in m=3; mode3 in m=4; mode4 in m=5) are significant different, as shear modes need more elements or higher-order kinematics to be simulated. However, axial and first bending modes modes are well described by lower-order beam models. The first eight modes of the single-bay box can be found in Fig. 13. It is interesting to note the capability of the present refined beam model to characterize warping phenomena.

6.6 Longeron

The cross-section of a typical longeron for aircraft and aerospace applications is shown in Fig. 14(a). The height of the cross-section is $a = 0.1$ m, with $a = b$. The distances between the flanges are $c = 0.04$ m and $d = 0.044$ m. The flanges' thicknesses are $t_1 = 0.01$ m and $t_2 = 0.002$ m. The length of the beam is equal to 1 m. The material is an aluminium alloy and its properties are as follows: Young modulus, $E = 75$ GPa; Poisson ratio, ν, is 0.33, material density $\rho = 2700$ kg/m^3. Three different LE models are considered in the following analysis, and the related cross-sectional discretizations are shown in Figs. 14(b) to 14(e).

Table 7 shows the first 8 frequencies (Hz) from m=1 to 5 by the present method and 3D FEM solution. Mode 1 is flexural for any value of m considered, and the data are in good agreement. The shell-like modes involving the vertical webs (see mode 6 and mode 7 in m=1; mode 4, mode 8 and mode 5 in m=3; mode 2, mode 3, mode 6 and mode 8 in m=4; mode 2, mode 3 and mode 8 in m=5) cannot be simulated via lower-order models. Some of these modes are shown in Fig. 15. In order to get those complex modes, higher-order kinematics (e.g., 20L9) is required. The first eight modes of the longeron can be found in Fig. 16.

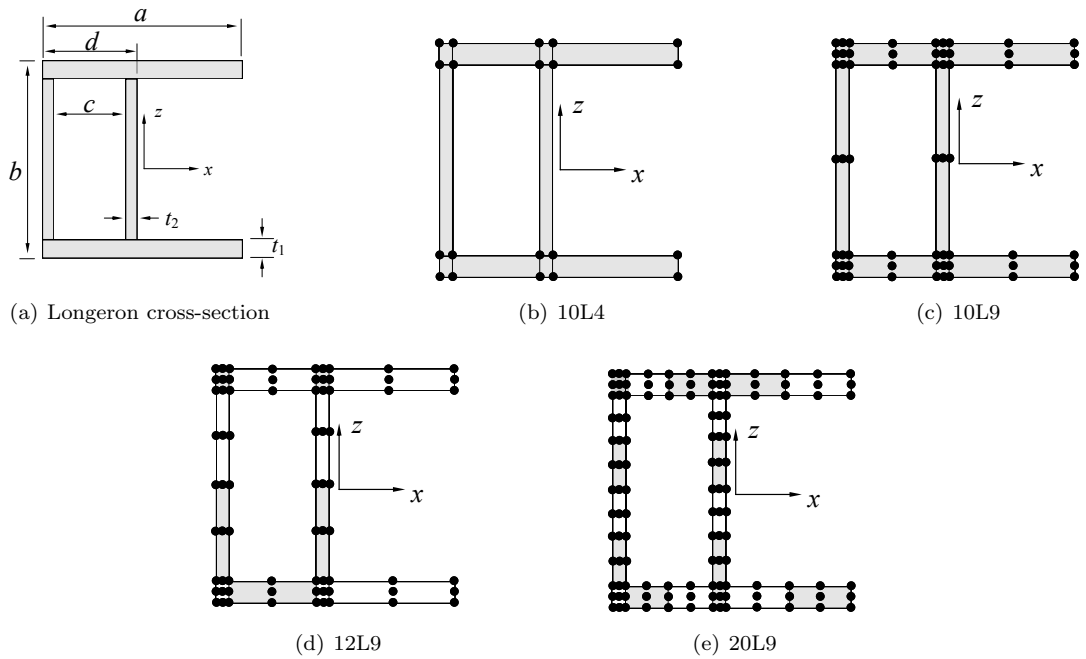

(a) Longeron cross-section (b) 10L4 (c) 10L9

(d) 12L9 (e) 20L9

Figure 14: Longeron cross-section and related LE discretizations.

Table 7: Natural frequencies (Hz) of the longeron for m=1 to 5

Cross-section			Natural Frequencies							
Seq.	Model	DOFs	Mode:1	2	3	4	5	6	7	8
	10L9	180	239.955	267.838	–[(a)]	–	1970.295	–	–	2633.401
	12L9	216	239.944	267.111	453.870	710.253	1965.180	–	–	2633.379
m=1	16L9	288	239.910	266.671	452.669	706.627	1827.561	–	–	2633.051
	20L9	360	239.765	266.461	424.326	700.119	1783.239	2005.077	2120.264	2633.458
	3D FEM	86160	239.709	266.210	414.390	695.480	1680.600	1796.400	1905.200	2633.200
	10L9		726.368	–	910.970	1589.623	2023.362	6387.458	–	6357.948
	12L9		707.237	886.127	910.515	1641.314	2018.076	5485.560	7208.783	5577.550
m=2	16L9		703.462	884.816	909.964	1632.712	1885.758	5306.938	6769.411	5167.075
	20L9		700.789	871.032	900.867	1631.367	1830.774	2021.908	2149.926	5094.411
	3D FEM		697.740	865.420	896.490	1625.800	1703.100	1830.000	1948.100	4586.200
	10L9		1204.834	2397.923	–	–	–	6391.168	2711.345	–
	12L9		1083.795	1674.159	–	–	–	6026.029	2691.325	–
m=3	16L9		1073.759	1671.977	–	–	–	5313.271	2674.125	–
	20L9		1069.993	1668.257	1713.209	1903.284	2085.039	2346.279	2671.897	5509.344
	3D FEM		1063.100	1598.500	1663.800	1731.200	1984.300	2208.800	2660.600	4703.000
	10L9		1608.210	–	–	2243.100	–	–	3836.262	–
	12L9		1434.678	–	–	2237.219	2645.275	–	3759.118	–
m=4	16L9		1417.275	–	–	2123.133	2639.702	–	3729.555	–
	20L9		1413.989	1955.761	1973.060	2203.398	2637.435	3338.458	3720.928	5981.294
	3D FEM		1403.000	1740.900	1763.400	2124.900	2626.000	3315.200	3680.600	4799.600
	10L9		1953.047	–	–	2415.473	3943.372	4355.915	–	–
	12L9		1780.258	–	–	2409.264	3661.489	4260.772	4857.956	–
m=5	16L9		1755.790	–	–	2305.875	3648.263	4221.106	4813.369	–
	20L9		1752.694	2014.223	2025.830	2360.688	3641.656	4687.170	4763.260	6316.506
	3D FEM		1736.900	1780.000	1802.700	2298.800	3608.800	4488.900	4673.400	4905.500

[(a)] Mode not provided by this model.

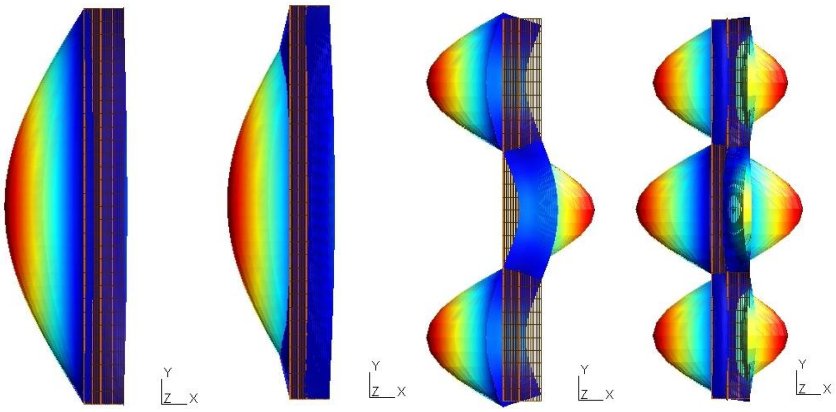

(a) m=1, mode6 (b) m=1, mode7 (c) m=3, mode3 (d) m=3, mode4

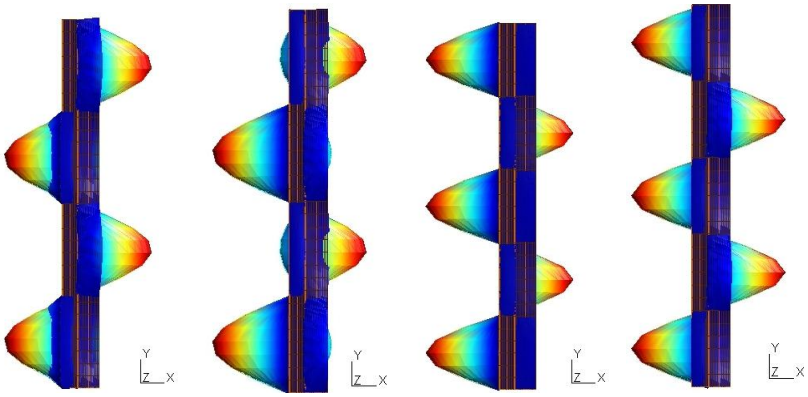

(e) m=4, mode2 (f) m=4, mode3 (g) m=5, mode2 (h) m=5, mode3

Figure 15: Shell-like modes of the vertical webs by the 20L9 model.

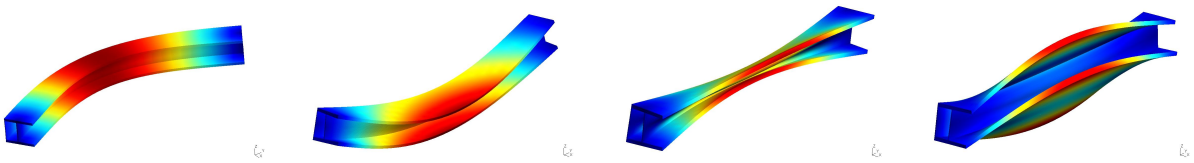

(a) m=1,f = 239.765Hz (b) m=1,f = 266.461Hz (c) m=1,f = 424.326Hz (d) m=1,f = 700.119Hz

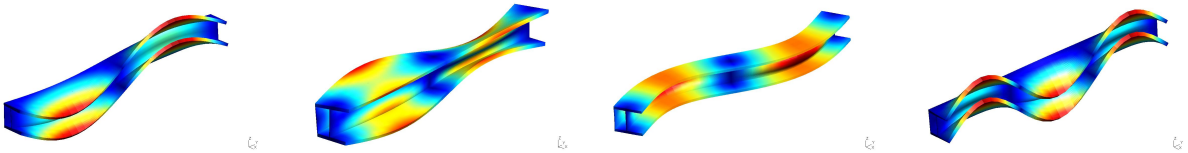

(e) m=2,f = 700.789Hz (f) m=2,f = 871.032Hz (g) m=2,f = 900.867Hz (h) m=3,f = 1069.993Hz

Figure 16: First eight modes of longeron by the 20L9 model.

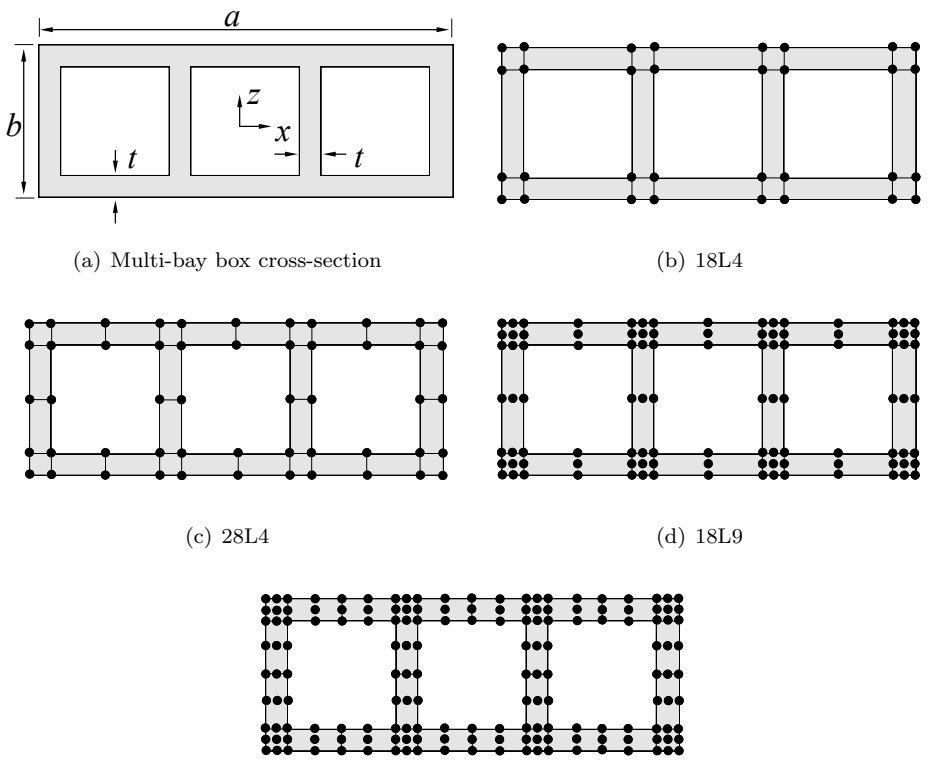

(a) Multi-bay box cross-section

(b) 18L4

(c) 28L4

(d) 18L9

(e) 28L9

Figure 17: Multi-bay box and related LE models.

6.7 Multi-bay box beam

As the final example, a multi-bay cross-section is studied as in Fig. 17(a). The dimensions of the cross-section are $a = 0.38$ m and $b = 0.14$ m. The thickness of the flanges are $t = 0.02$ m, and the whole length of this beam is $L = 10a$. The material data are as in the previous analysis case. Four different LE discretizations are shown in Figs. 17(b) to 17(e).

Table 8 shows the natural frequencies for the structure under analysis by the present beam theories and the 3D FEM code Nastran. The modes in column 4 are flexural along the axis ox, while those in column 5 are flexural modes along the axis oz. The first torsional modes can be found in column 6. From m=3 to m=5, the sequences of some modes are interchanged (see mode 4 to mode 6 in m=3; mode 4 to mode 7 in m=4; mode 6 and mode 7 in m=5). Mode 6 in m=3 and mode 7 in m=4 are axial modes (see Fig. 18). Those kind of modes generally need a fewer DOFs to be detected. Attention should be paid to mode 7 in m=5 (see Fig. 18(d)), which, although extensional, need refined kinematics to be described. Higher order torsional modes (see mode 4 in m=3; mode 4 and mode 6 in m=4; mode 6 in m=5) need more L9 elements to be simulated. In the last column of Table 8, the modes are characterized by severe cross-sectional distortions; thus, higher-order models are strictly needed in this case. Figure 19 finally shows the first eight modes of the multi-bay beam by the higher-order 28L9 1D model.

Table 8: Natural frequencies of the multi-bay box for m=1 to 5

Cross-section			Natural Frequencies							
Seq.	Model	DOFs	Mode:1	2	3	4	5	6	7	8
	18L4	96	29.777	66.688	282.761	693.051	2974.623	3571.696	5389.380	–[(a)]
	24L4	156	29.551	66.517	281.994	693.045	2296.060	2638.059	4048.432	–
m=1	18L9	306	29.468	66.174	281.254	693.046	1951.766	2426.413	3407.737	–
	28L9	486	29.435	66.426	276.265	693.042	1484.597	1663.744	2446.303	3406.351
	3D FEM	86160	29.435	66.420	275.050	693.030	1406.300	1562.300	2316.100	3317.300
	18L4		117.164	250.617	563.121	1383.403	3016.660	3601.175	5410.071	–
	24L4		116.223	249.470	557.610	1383.338	2343.319	2684.732	4075.922	–
m=2	18L9		115.818	248.113	554.541	1383.324	2002.634	2475.217	3435.834	–
	28L9		115.671	248.763	534.016	1383.274	1544.455	1741.144	2486.853	3415.965
	3D FEM		115.670	248.670	528.870	1383.200	1468.000	1644.500	2358.200	3358.600
	18L4		256.813	517.334	839.088	3086.210	3654.676	2067.689	5445.293	–
	24L4		254.551	513.677	821.437	2420.665	2768.672	2067.345	4122.298	–
m=3	18L9		253.374	510.630	813.002	2085.226	2563.794	2067.152	3481.711	–
	28L9		433.169	511.195	758.925	1639.867	1883.045	2066.838	2554.312	3432.216
	3D FEM		252.950	510.810	745.630	1565.800	1795.800	2066.300	2427.900	2734.700
	18L4		441.201	834.969	1109.511	3182.244	3737.223	5495.856	2740.834	–
	24L4		436.805	826.956	1070.480	2525.977	2895.913	4188.080	2739.427	–
m=4	18L9		434.119	821.444	1052.878	2196.512	2698.815	3543.026	2738.103	–
	28L9		426.923	821.010	950.280	1765.634	2092.864	2648.095	2736.404	3455.948
	3D FEM		433.070	819.960	926.820	1694.000	2017.600	2524.600	2734.700	3345.700
	18L4		662.051	1181.709	1374.474	3303.140	3853.311	5562.491	–	–
	24L4		654.458	1167.499	1305.709	2656.543	3069.629	4273.574	–	–
m=5	18L9		649.234	1158.511	1275.770	2332.967	2882.757	3617.133	3378.473	–
	28L9		647.287	1123.914	1155.947	1916.425	2358.725	2767.188	3361.402	3502.110
	3D FEM		646.960	1092.400	1153.700	1846.900	2293.600	2647.100	3450.400	3613.900

[(a)] Mode not provided by this model.

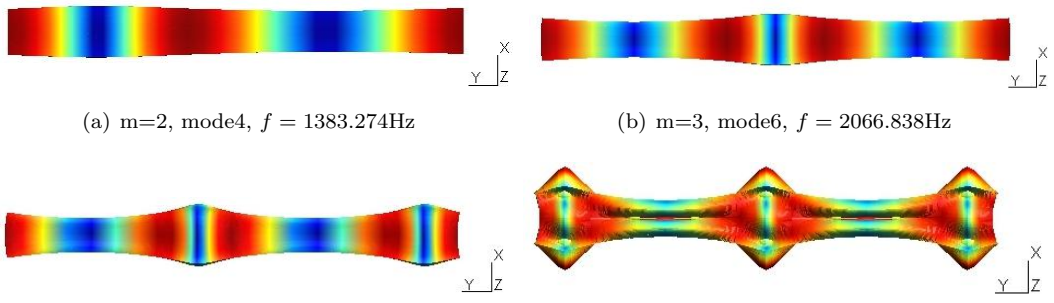

(a) m=2, mode4, $f = 1383.274$Hz

(b) m=3, mode6, $f = 2066.838$Hz

(c) m=4, mode7, $f = 2736.404$Hz

(d) m=5, mode7, $f = 3361.402$Hz

Figure 18: Axial modes by the 28L9 model from top view.

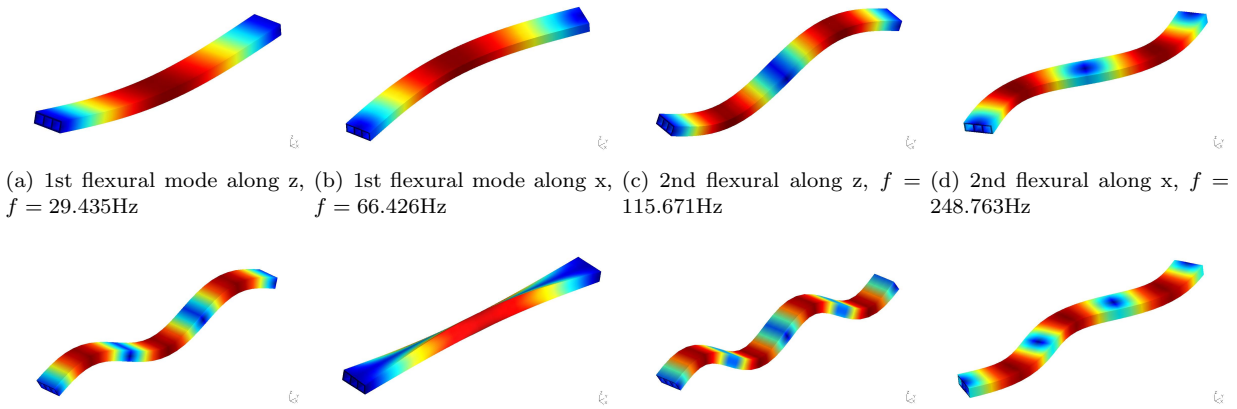

(a) 1st flexural mode along z, $f = 29.435$Hz (b) 1st flexural mode along x, $f = 66.426$Hz (c) 2nd flexural along z, $f = 115.671$Hz (d) 2nd flexural along x, $f = 248.763$Hz

(e) 3rd flexural along z, $f = 252.966$Hz (f) 1st torsional, $f = 276.265$Hz (g) 4th flexural along z, $f = 433.169$Hz (h) 3rd flexural along x, $f = 511.195$Hz

Figure 19: First eight modes of the multi-bay box by the 28L9 model.

7 Conclusions

Higher-order models for the analysis of the free vibrations of simply-supported beams have been proposed in this paper. By exploiting the Carrera Unified Formulation (CUF) and Lagrange polynomials to discretize the beam cross-sectional kinematics, refined models with only displacement variables have been developed. The governing differential equations have been formulated in strong form by using the principle of virtual displacement. Subsequently, by assuming simply supported boundary conditions, analytical solutions of arbitrarily refined beam models have been devised. Both short and long beams have been addressed to verify the refined beam models. Four-point (L4), nine-point (L9) and sixteen-point (L16) Lagrange polynomials have been used to investigate square, C-shaped, Z-shaped, I-shaped, single box-, longeron- and multi-box- cross-sections. Two different ways have been addressed in the present LE formulation in order to improve the accuracy of the beam theory:

1. By increasing the order of cross-sectional Lagrange polynomial expansions (i.e., L4, L9, and L16);

2. By increasing the number of elements of the cross-section.

Using those approaches, higher order models that are able to deal with shear deformation and higher-order effects such as warping, can be captured straightforwardly with the help of CUF. The following considerations arise from the comparison of the present approach with results available in the literature and 3D FEM solutions from commercial code:

1. The Lagrange-based formulation has enhanced capabilities compared to Talyor-based CUF modelling. The higher the Lagrange polynomials order, the better the accuracy.

2. The mode appearance can be interchanged in lower-order LE models (L4), even if a large number of elements on the cross-section are used. By using higher Lagrange polynomials (L9 or L16) with fewer elements, interchange can also be shown.

3. Axial modes need a few DOFs (no matter L4 or L9) in the case of lower m. On the contrary, even for axial modes, higher-order models are needed for higher m values.

4. Lower-order models give good results in the case of symmetrical cross-section (e.g., I-shaped, single-bay box shape, multi-bay box shape). On the other hand, the analysis of non-symmetrical structures demands for the use of refined beam models with a large number of Lagrange elements. Non-symmetric structures require higher-order Lagrange expansion with a large number of elements.

5. For all the problem considered, the present analytical LE formulation clearly demonstrates its efficiency over 3D FEM solutions and the capabilities of capturing higher-order refined effects.

Acknowledgments

The first author acknowledges China Scholarship Council and the basic scientific research colleges in CAUC (No.:3122014D014).

References

[1] L. Euler. *De curvis elasticis*. Lausanne and Geneva: Bousquet, 1744.

[2] D. Bernoulli. De vibrationibus et sono laminarum elasticarum. *In:Commentarii Academiae Scientiarum Imperialis Petropolitanae*, Petropoli, 1751.

[3] A. de Saint-Venant. Mémoire sur la flexion des prismes. *Journal de Mathématiques pures et appliqués*, 1:89–189, 1856a.

[4] A. de Saint-Venant. Mémoire sur la torsion des prismes. *Académie des Sciences de l'Institut Impérial de Frances*, 14:233–560, 1856b.

[5] S.P. Timoshenko. On the corrections for shear of the differential equation for transverse vibrations of prismatic bars. *Philosophical Magazine*, 41:744–746, 1921.

[6] S.P. Timoshenko. On the transverse vibrations of bars of uniform cross section. *Philosophical Magazine*, 43:125–131, 1922.

[7] E. Carrera, G. Giunta, and M. Petrolo. *Beam Structures: Classical and Advanced Theories*. John Wiley & Sons, 2011.

[8] K. Kapania and S. Raciti. Recent advances in analysis of laminated beams and plates, part I: Shear effects and buckling. *AIAA Journal*, 27(7):923–935, 1989.

[9] K. Kapania and S. Raciti. Recent advances in analysis of laminated beams and plates, part II: Vibrations and wave propagation. *AIAA Journal*, 27(7):935–946, 1989.

[10] E. Carrera, A. Pagani, M. Petrolo, and E. Zappino. Recent developments on refined theories for beams with applications. *Mechanical Engineering Reviews*, 2(2), 2015.

[11] I.S. Sokolnikoff. *Mathematical Theory of Elasticity.* Mcgrw-Hill, 1956.

[12] S. P. Timoshenko and J. N. Goodier. *Theory of elasticity.* McGraw-Hill, 1970.

[13] F. Gruttmann, R. Sauer, and W. Wagner. Shear stresses in prismatic beams with arbitrary cross-sections. *International Journal for Numerical Methods in Engineering*, 45:865–889, 1999.

[14] F. Gruttmann and W. Wagner. Shear correction factors in timoshenko's beam theory for arbitrary shaped cross-sections. *Computational Mechanics*, 27:199–207, 2001.

[15] W. Wagner and F. Gruttmann. A displacement method for the analysis of flexural shear stresses in thin-walled isotropic composite beams. *Computers and Structures*, 80(24):1843–1851, 2002.

[16] P. Ladéveze and J. Simmonds. De nouveaux concepts en théorie des poutres poutres pour des charges et des géométries quelconques. *Comptes Rendus Acad. Sci. Serie IIc, Paris*, 322(6):445–462, 1996.

[17] P. Ladéveze and J. Simmonds. New concepts for linear beam theory with arbitary geometry and loading. *European Journal of Mechanics-A/Solids*, 17(3):377–402, 1998.

[18] P. Ladéveze, Ph. Sanchez, and J.G. Simmonds. Beamlike(saint-venant) solutions for fully anisotropic elastic tubes of arbitrary closed cross section. *Internatinal Journal of Solids and Structures*, 41(7):1925–1944, 2004.

[19] W. Yu, V.V. Volovoi, D.H. Hodges, and X. Hong. Validation of the variational asymptotic beam sectional analysis. *AIAA Journal*, 40(10):2105–2113, 2002.

[20] W. Yu and D. H. Hodges. Elasticity solutions versus asymptotic sectional analysis of homogeneous, isotropic, prismatic beams. *Journal of Applied Mechanics*, 71:15–23, 2004.

[21] W. Yu and D. H. Hodges. Generalized timoshenko theory of the variational asymptotic beam sectional analysis. *Journal of the American Helicopter Society*, 50(1):46–55, 2005.

[22] R. El Fatmi. Non-uniform warping including the effects of torsion and shear forces. Part I: A general beam theory. *International Journal of Solids and Structures*, 44(18–19):5912–5929, 2007.

[23] R. El Fatmi. Non-uniform warping including the effects of torsion and shear forces. Part II: Analytical and numerical applications. *International Journal of Solids and Structures*, 44(18–19):5930–5952, 2007.

[24] J.N. Reddy. On locking-free shear deformable beam finite elements. *Computer methods in applied mechanics and engineering*, 149:113–132, 1997.

[25] J.N. Reddy. *Mechanics of laminated composite plates and shells. Theory and Analysis*. CRC Press, 2^{nd} edition, 2004.

[26] M. Eisenberger, H. Abramovich, and O. Shulepov. Dynamic stiffness analysis of laminated beams using a first order shear deformation theory. *Composite Structures*, 31(4):265–271, 1995.

[27] S.R. Marur and T. Kant. Free vibration analysis of fiber reinforced composite beams using higher order theories and finite element modelling. *Journal of Sound and Vibration*, 194(3):337–351, 1996.

[28] S.R. Marur and T. Kant. On the angle ply higher order beam vibrations. *Computational Mechanics*, 40(1):25–33, 2007.

[29] R. Ganesan and A. Zabihollah. Vibration analysis of tapered composite beams using a higherorder finite element. part i: Formulation. *Composite Structures*, 77(3):306–318, 2007.

[30] R. Ganesan and A. Zabihollah. Vibration analysis of tapered composite beams using a higherorder finite element. part i:parametric study. *Composite Structures*, 77(3):319–330, 2007.

[31] M. Kameswara Rao, Y.M. Desai, and M.R. Chitnis. Free vibrations of laminated beams using mixed theory. *Composite Structures*, 52(2):149–160, 2001.

[32] E. Carrera. Theories and finite elements for multilayered, anisotropic, composite plates and shells. *Archives of Computational Methods in Engineering*, 9(2):87–140, 2002.

[33] E. Carrera. Theories and finite elements for multilayered plates and shells: a unified compact formulation with numerical assessment and benchmarking. *Archives of Computational Methods in Engineering*, 10(3):216–296, 2003.

[34] E. Carrera and S. Brischetto. Analysis of thickness locking in classical, refined and mixed multilayered plate theories. *Composite Structures*, 82(4):549–562, 2008.

[35] E. Carrera and G. Giunta. Refined beam theories based on a unified formulation. *International Journal of Applied Mechanics*, 2(1):117–143, 2010.

[36] E. Carrera, G. Giunta, P. Nali, and M. Petrolo. Refined beam elements with arbitrary cross-section geometries. *Computers and Structures*, 88(5–6):283–293, 2010.

[37] E. Carrera, M. Petrolo, and P. Nali. Unified formulation applied to free vibrations finite element analysis of beams with arbitrary section. *Shock and Vibrations*, 18(3):485–502, 2011.

[38] E. Carrera and M. Filippi. Variable kinematic one-dimensional finite elements for the analysis of rotors made of composite materials. *Journal of Engineering for Gas Turbines and Power*, 136(9):092501, 2014.

[39] G. Giunta, F. Biscani, S. Belouettar, and E. Carrera. Analysis of thin-walled beams via a one-dimensional unified formulation through a navier-type solution. *International Journal of Applied Mechanics*, 3(3):407–434, 2011.

[40] A. Pagani, M. Boscolo, J.R. Banerjee, and E. Carrera. Exact dynamic sitffness elements based on one-dimensional higher-order theories for free virbation anaylsis of solid and thin-walled structures. *Journal of Sound and Virbration*, 332(23):6104–6127, 2013.

[41] A. Pagani, E. Carrera, M. Boscolo, and J.R. Banerjee. Refined dynamic stiffness elements applied to free vibration analysis of generally laminated composite beams with arbitrary boundary conditions. *Composite Structures*, 110:305–316, 2014.

[42] E. Carrera and M. Petrolo. Refined one-dimensional formulations for laminated structure analysis. *AIAA journal*, 50(1):176–189, 2012.

[43] E. Carrera and M. Petrolo. Refined beam elements with only displacement variables and plate/shell capabilities. *Meccanica*, 47(3):537–556, 2012.

[44] E. Carrera, A. Pagani, and M. Petrolo. Classical, refined, and component-wise analysis of reinforced-shell wing structures. *AIAA Journal*, 51(5):1255–1268, 2013.

[45] S.W. Tsai and T.N. Massard. *Composites Design*. Dayton, Think Composites, 4th edition, 1988.

[46] E. Carrera, S. Brischetto, and P Nali. *Plates and Shells for Smart Structures: Classical and Advanced Theories for Modeling and Analysis*. John Wiley & Sons, 2011.

[47] E. Carrera, M. Cinefra, E. Zappino, and M. Petrolo. *Finite Element Analysis of sutructures through unified formulation*. John Wiley & Sons, 2014.

[48] MSC. Software Corporation. *MD Nastran 2010 Quick Reference Guide*. 2010.